Tectonophysics 530–531 (2012) 225–239

Contents lists available at SciVerse ScienceDirect

Tectonophysics

journal homepage: www.elsevier.com/locate/tecto

Modern seismological reassessment and tsunami simulation of historical Hellenic Arc earthquakes

C.W. Ebeling [a,*], E.A. Okal [a], N. Kalligeris [b], C.E. Synolakis [c,d]

[a] Department of Earth and Planetary Sciences, Northwestern University, 1850 Campus Drive, Evanston, IL 60208, USA
[b] Technical University of Crete, Chanea, Crete 73100, Greece
[c] Department of Civil Engineering, University of Southern California, Los Angeles, CA 90089, USA
[d] Hellenic Center for Marine Research, Anavyssos 19013, Greece

ARTICLE INFO

Article history:
Received 26 May 2011
Received in revised form 20 December 2011
Accepted 23 December 2011
Available online 2 January 2012

Keywords:
Earthquake
Hazard
Hellenic Arc
Magnitude
Relocation
Tsunami

ABSTRACT

Neither large magnitude nor tsunamigenic earthquakes occur frequently in the eastern Mediterranean, hampering comprehensive study of these events and consequential hazards whenever digital data are required. Using analog seismograms, travel-time catalogs, and hydrodynamic simulations, we reassess here four large ($M\sim7$) historical earthquakes occurring in various regions of the Hellenic Arc: on 6 October 1947, in the Peloponnesus; 9 February 1948, near Karpathos; and a couplet east of Rhodos on 24 and 25 April 1957. Damaging near-field tsunamis are associated with the 1947 and 1948 earthquakes. Results include seismic moments (in units of 10^{27} dyn·cm) of 1.26 (1947), 0.97 (1948), 0.56 (1957a), and 1.09 (1957b); recovered focal mechanisms and hypocentral locations are consistent with the regional stress field resulting from the ongoing collision between the Nubia plate and Aegea microplate. Seismological reassessments indicate that the sources of the 1947 and 1948 tsunamis involved submarine slumping; hydrodynamic simulations assuming a submarine landslide source for the 1948 tsunami recreate run-up and inundation values consistent with eyewitness accounts presented here. Hydrodynamic simulations also show that the 25 April 1957 earthquake likely generated an unobserved tsunami with a maximum 50 cm run-up in Rhodos.

© 2011 Elsevier B.V. All rights reserved.

1. Introduction

Comprehensive understanding of large tsunamigenic eastern Mediterranean earthquakes and consequential tsunami hazard is hindered by the absence of such events after digital recording began in the 1980s. Using analog seismograms, Okal et al. (2009) studied the 1956 Amorgos earthquake, the largest to affect Greece during the last 100 years, and its associated tsunami. Here we extend their work to four other large Hellenic Arc earthquakes: in the southwestern Peloponnesus on 6 October 1947, near Karpathos on 9 February 1948, and two east of Rhodos on 24 and 25 April 1957 (Fig. 1(b)); these represent the only other shallow (h<70 km) events in the Aegean region assigned a Pasadena magnitude M_{PAS} greater than $6\frac{7}{8}$ as defined by Gutenberg and Richter (1954).

Significant tsunamis were associated with the events of 1947 and 1948. While the targeted events have been mentioned in previous seismological studies (e.g. Abe, 1981; Ambraseys, 2001; Ambraseys and Jackson, 1990; Gutenberg and Richter, 1954; Makropoulos, 1978; McKenzie, 1972; Papazachos and Delibasis, 1969; Ritsema, 1974), our reassessment of these earthquakes is motivated both by the scatter in published locations, depths, and focal geometries, and by the absence of seismic moments obtained using modern seismological techniques.

A notable gap also exists in the understanding of the 1947 and 1948 tsunamis, and of these four earthquakes as tsunami sources. We address this by using hydrodynamic simulations based on our seismological reassessments; run-up and inundation measurements based on eyewitness accounts further constrain our 1948 tsunami simulation. Even though no tsunami has been linked to either 1957 earthquake, these events may have been large enough to generate observable tsunamis on Rhodos and perhaps on the southwest coast of Turkey.

1.1. Tectonic setting

The eastern Mediterranean region (Fig. 1(a)) contains the Anatolia, Arabia, and Nubia plates, and the Aegea microplate, which moves 30±1 mm/yr to the southwest relative to Eurasia (McClusky et al., 2000, 2003) and at a slightly lower velocity to the southwest relative to Nubia (Kreemer and Chamot-Rooke, 2004; Reilinger et al., 2006). Major regional tectonic features include the 9±1 mm/yr left-lateral strike-slip East Anatolia Fault in eastern Turkey (McClusky et al., 2000, 2003) and the 24±1 mm/yr right-lateral strike-slip North Anatolia Fault in northern Turkey (McClusky et al., 2000, 2003). The system is dominated by the Hellenic Arc and trench

* Corresponding author. Tel.: +1 847 467 1639; fax: +1 847 491 8060.
E-mail address: carl@earth.northwestern.edu (C.W. Ebeling).

0040-1951/$ – see front matter © 2011 Elsevier B.V. All rights reserved.
doi:10.1016/j.tecto.2011.12.036

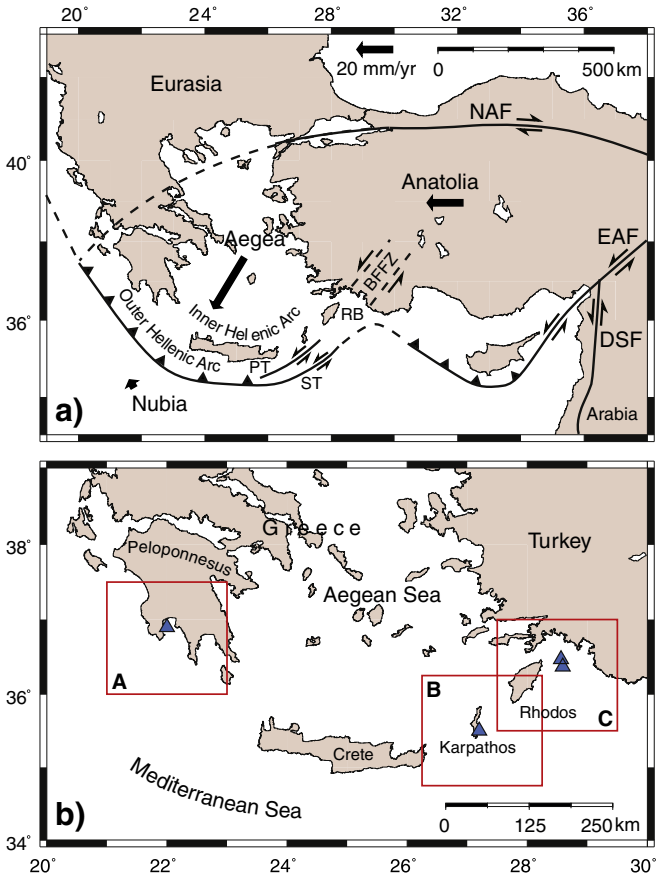

Fig. 1. (a) Simplified tectonic map showing the eastern Mediterranean region, after Hall et al. (2009), Jackson (1994), Jongsma (1977), McClusky et al. (2000, 2003), and Reilinger et al. (2006). BFFZ = Burdur-Fethiye Fault Zone; DSF = Dead Sea Fault; EAF = East Anatolian Fault; PT = Pliny Trench; RB = Rhodos Basin; ST = Strabo Trench. Lines indicate faults (dashed when inferred). Teeth on overriding plate show thrust fault; sense of motion shown by half-arrows when strike-slip. Solid arrows show velocities relative to Eurasia. (b) Map showing International Seismological Summary (ISS) locations of events included in this study. Box A: 6 October 1947 event; B: 9 February 1948; C (south): 24 April 1957; and C (north): 25 April 1957. Areas outlined in red correspond to maps in Figs. 3(a), 4(a), 5(a), and 6(a).

(LePichon and Angelier, 1979), along which Nubia Neo-Tethys oceanic lithosphere subducts northward under southern Aegea.

Aegea tectonics are characterized by 35–40 mm/yr north–south extension in central and southern Aegea (Kiratzi and Louvari, 2003; Kiratzi and Papazachos, 1995; LePichon and Angelier, 1979; McClusky et al., 2000; McKenzie, 1978); east–west extension in the inner Hellenic Arc (Kreemer and Chamot-Rooke, 2004; McClusky et al., 2003); and thrust faulting in the outer Hellenic Arc (Benetatos et al., 2004; McKenzie, 1972, 1978). Roll-back of the subducting Nubia slab plays an influential kinematic role by inducing Aegea to move towards the Hellenic trench (Bohnhoff et al., 2005; Reilinger et al., 2006).

Nubia-Aegea relative plate motion at the Hellenic Arc, directed ~N45°E (Bohnhoff et al., 2005), results in convergence varying from nearly arc-orthogonal in the west to left-lateral arc-oblique in the east. While evidence exists for large vertical displacements across the northeast–east–northeast-trending deep-sea depressions on the eastern limb of the arc known as the Pliny and Strabo trenches (Jongsma, 1977), it is primarily left-lateral strike-slip motion arising from arc-oblique convergence that is accommodated by these structures (Kreemer and Chamot-Rooke, 2004; LePichon and Angelier, 1979; LePichon et al., 1995). The western terminus of the Pliny and Strabo trenches lies southeast of Crete. While their eastern terminations are not well defined, a broad Pliny-Strabo zone of deformation has been correlated with the Burdur-Fethiye Fault Zone in southwestern Turkey (Hall et al., 2009).

2. Methodologies and data sets

2.1. Event relocation

We used the interactive and iterative Monte Carlo relocation algorithm of Wysession et al. (1991) to relocate events. Relocations were carried out using *P*-wave arrival time data published by the International Seismological Summary (ISS) from stations located at epicentral distances up to 100° (Table 1). Uncertainties in relocation arise from station timing errors and bias in station coverage, which is best in the east and northeast, where stations located in Japan and east Asia dominate; and in the northwest quadrant, where a large number of stations in Europe and North America are located. To replicate timing uncertainties typical of the 1940s and 1950s, randomly-generated Gaussian noise (σ_G=3–5 s) was included in arrival time data sets. The resulting 95% confidence ellipse expresses a relocation's reliability.

2.2. Preliminary determination of focal mechanism (PDFM) inversion

To recover fault plane solutions and seismic moments, we used the Preliminary Determination of Focal Mechanism (PDFM) method (Reymond and Okal, 2000), which inverts mantle Rayleigh and Love wave spectral amplitudes. This method is ideal for use with sparse data sets made up of historical records in that it does not rely on erroneous or non-existent time corrections and instrument polarities. It is robust for data sets consisting of only a few records, given sufficient azimuthal coverage (Reymond and Okal, 2000), and is largely insensitive to uncertainties in epicentral estimates (Okal and Reymond, 2003). But because the PDFM algorithm does not use phase information (Okal and Reymond, 2003; Reymond and Okal, 2000; Romanowicz and Suárez, 1983), it results in indeterminacies in fault strike φ, in which the entire fault plane solution can be rotated 180° in the horizontal plane, and in the sense of slip on the fault, which can be reversed by adding 180° to the slip angle λ while fault strike φ and dip δ remain the same.

Indeterminacies were resolved using body-wave polarities and relative amplitudes recorded at the stations used in PDFM inversions and at De Bilt, Netherlands (DBN) and Vienna, Austria (VIE). Seismograms from these regional stations were not used in inversions because epicentral distances did not allow sufficient temporal separation of Love and Rayleigh wavetrains.

Centroid depths for these events were obtained by minimizing root-mean-square residuals of PDFM inversions at depths constrained between 10 and 100 km.

The analog seismograms came from the Benioff 1–90 seismometer at Pasadena, California (PAS); the McRomberg tilt-compensating seismometer at College, Alaska (COL); the Milne-Shaw seismometer at Honolulu, Hawaii (HON); and Wenner seismometers at Huancayo, Peru (HUA) and San Juan, Puerto Rico (SJG) (Fig. 2). High-quality first-passage Love (G_1) and Rayleigh (R_1) wavetrains in these seismograms were digitized and equalized to a 1 Hz sampling rate. Digitized records were corrected for instrument response, magnification, and damping, using instrument constants as described in Charlier and van Gils (1953). Stations used in PDFM inversions are listed in Table 2.

3. Results

3.1. Southwest Peloponnesus, 6 October 1947 (1947:279)

3.1.1. Background and previous work

The earthquake of October 6, 1947 resulted in severe damage, three deaths, and over 20 injuries in the southwestern Peloponnesus Galanopoulos (1949). A tsunami associated with this event inundated Methoni, a coastal town on the Mediterranean Sea, from 15 m to 60 m

Download English Version:

https://daneshyari.com/en/article/6434273

Download Persian Version:

https://daneshyari.com/article/6434273

Daneshyari.com